Highly Efficient Light-Driven CO 2 to CO Reduction by an Appropriately Decorated Iron Porphyrin Molecular Catalyst

Aspasia Stoumpidi, Adelais Trapali, Marie Poisson, Alexandre Barrozo, Sylvain Bertaina, Maylis Orio, Georgios Charalambidis, Athanassios Coutsolelos

Highly Efficient Light-Driven CO_2 to CO reduction by an Appropriately Decorated Iron Porphyrin Molecular Catalyst

Aspasia Stoumpidi,[1] Adelais Trapali,[1] Marie Poisson,[2] Alexandre Barrozo,[2] Sylvain Bertaina,[3] Maylis Orio,[2] Georgios Charalambidis,*[1] Athanassios G. Coutsolelos*[1]

[1]*Department of Chemistry, University of Crete, Laboratory of Bioinorganic Chemistry, Voutes Campus, Heraklion 70013, Crete, Greece. e-mail:* acoutsol@uoc.gr, gcharal@uoc.gr

[2]*Aix Marseille Université, CNRS, Centrale Marseille, iSm2, Marseille 13397, France.*

[3] *Aix-Marseille Université, CNRS, IM2NP UMR 7334, Marseille 13397, France.*

ABSTRACT

The photocatalytic CO_2 reduction into value-added chemicals is regarded as one promising technology to mitigate environmental issues and the energy crisis of the modern world due to the extended CO_2 emissions. Recent advances have shown that iron porphyrins are considered as one of the most efficient molecular catalysts in the activation and reduction of molecules like CO_2. Thus, we have prepared a suitably modified Fe^{III} porphyrin (**$[Fe^{III}(TF_4TMAP)](CF_3SO_3)_5$**) and studied its catalytic activity in terms of photocatalytic reduction of CO_2. This iron catalyst possesses four fluorine substituents in the *ortho* and the *meta* position of each *meso*-phenyl group of the porphyrin, while trimethyl-ammonium groups were placed in the *para* position. Photocatalytic studies were performed in the presence of an iridium complex as a chromophore and have shown that **$[Fe^{III}(TF_4TMAP)](CF_3SO_3)_5$** can effectively reduce CO_2, achieving excellent turnover numbers (up to 5500 TONs) and high turnover frequencies. The main reduction product of this photocatalytic system was

CO, and only a small amount of hydrogen was detected, presenting a maximum selectivity of 86% for CO.

INTRODUCTION

Over the past decades, the energy consumption increased dramatically, and along with the extensive use of fossil fuels as the primary energy source, various gaseous pollutants have been emitted into the atmosphere, especially CO_2.[1] CO_2 is one of the greenhouse gases, and the substantial rise in CO_2 emissions, is responsible for many of the global-warming related environmental problems.[2] Therefore, effective CO_2 utilization and conversion into value-added chemicals are regarded as one of the most promising strategies to overcome these phenomena and realize an energy-sustainable society. Over the last few decades, a great amount of appropriate catalysts that can perform CO_2 reduction to CO, HCOOH, CH_4, CH_3OH, etc., have been developed.[3] Moreover, for the transformation of CO_2 several elecrochemical[3a, 4], or photo-initiated methods[5] were employed. However, photochemical conversion, inspired by natural photosynthesis, is considered as the most viable solution since solar light is abundant and ecofriendly.[6] Therefore, reduction of CO_2 is a fruitful approach for storing the renewable solar energy into the chemical bonds of value-added chemicals. There are several approaches to developing systems capable of catalyzing CO_2 reduction under light irradiation.[7] Nevertheless, the design of low-cost molecular catalysts with high catalytic activity and stability remains challenging. In addition, the selectivity over the CO_2 reduction products is another crucial issue to be addressed. The competitive formation of hydrogen is kinetically favored in the presence of H_2O[8] and influences the efficiency of CO_2 conversion depending on the catalytic conditions as well as the catalyst and the photosensitizer (PS).

In homogenous photocatalytic systems, a photosensitizer, a catalyst, and a sacrificial electron donor (SED) are the three basic components.[9] In most photocatalytic systems, the PS can photochemically mediate the electron transfer from a reductant species known as the SED, to the catalyst. Depending on the catalyst, the accumulated electrons are then introduced to the CO_2 molecule, which is converted to another product.[10] Among the various molecular catalysts reported in electro- and photo-catalysis, only a few can produce highly reduced hydrocarbons derived from CO_2.[11] In general, the process of CO_2 reduction can lead in the formation of carbon monoxide, formic acid, formaldehyde, methane etc., depending on the nature of the catalyst.[9] However, most of the catalysts yield mainly CO or HCOOH, since their formation requires a two-electron/proton process and thereby the minimal energy is

needed.[12] CO albeit is known to be toxic, it is of great industrial importance for the production of useful chemicals or other valuable products. It can be used either as a pure compound or as a mixture combined with H_2 for the preparation of various chemical products via Fischer–Tropsch chemistry.[13]

Numerous approaches have been effectively established in developing metal-based molecular catalysts. The majority of them include expensive noble metals, such as rhenium[14] or iridium,[15] and only few of them are based on earth abundant elements, such as manganese,[16] copper,[17] cobalt[18] and iron.[19] Iron porphyrins is a promising family of catalysts based on noble free metal, and present effective activity for both electrochemical and photochemical reduction of CO_2.[20], [21] Almost in every catalytic CO_2 reduction system, the key steps are the activation of the metal center within the catalyst and then CO_2 coordination. Iron porphyrins can accept and accumulate electrons from the PS, resulting in CO_2 stabilization and binding on the metal.[10] Thus, in this case, the factor that can promote the catalytic process is the three-electron reduction of Fe^{III} to the formal active Fe^0 state, in which CO_2 coordinates on the iron metal center.[22]

Plenty of publications describe CO_2 activation and reduction applying iron porphyrins as catalysts.[23] Moreover, recent advances suggest that the secondary sphere of the porphyrin influences the catalytic efficiency.[24] CO_2 conversion can be improved by introducing electron-donating and positively charged functional groups at the periphery of the porphyrin macrocycle.[25] In detail, the secondary coordination sphere stabilizes more effectively the CO_2 onto the metal center, which is typically the rate determining step during the reduction process.[26]

In this work, we describe the visible light-driven CO_2 to CO reduction, using for the first time the iron porphyrin derivative **$[Fe^{III}(TF_4TMAP)](CF_3SO_3)_5$** (Figure 1) as molecular catalyst. The selected iron catalyst possesses four fluorine substituents in the *ortho* and the *meta* position of each *meso*-phenyl group of the porphyrin. The electron-withdrawing nature of fluorine groups is expected to shift the standard potential of the catalyst toward positive values. This will facilitate the reduction of iron to the formal Fe^0 state, which is a prerequisite process before the coordination of CO_2 to the iron center.[27] Additionally, positively charged trimethyl-ammonium groups were placed in the *para* position of each phenyl to promote the CO_2

stabilization on the metal center.[28] The positively charged groups can provide stabilization towards CO_2 coordination by through-space interactions, leading to enhanced catalytic activity.[29] To verify the importance of fluorine substituents and the positively charged trimethyl-ammonium groups, the catalytic activity of three reference iron catalysts (**[Fe^{III}(TF$_5$PP)]Cl**, **[Fe^{III}(TF$_4$-DMAP)]Cl** and **[Fe^{III}(TMAP)]Cl$_5$**, Figure 1) was also examined. It's worth mentioning that porphyrin **[Fe^{III}(TMAP)]Cl$_5$** has been studied extensively by the group of Robert,[30] presenting high catalytic activity.

The photocatalytic experiments demonstrated that **[Fe^{III}(TF$_4$TMAP)](CF$_3$SO$_3$)$_5$** is a very efficient catalyst, achieving extremely high CO_2 to CO reduction activity (TON_{CO} = 5500, TOF_{CO} = 1375 h^{-1}) in the presence of **[Ir(ppy)$_2$bpy]PF$_6$** as PS and triethylamine (TEA) as sacrificial electron donor.

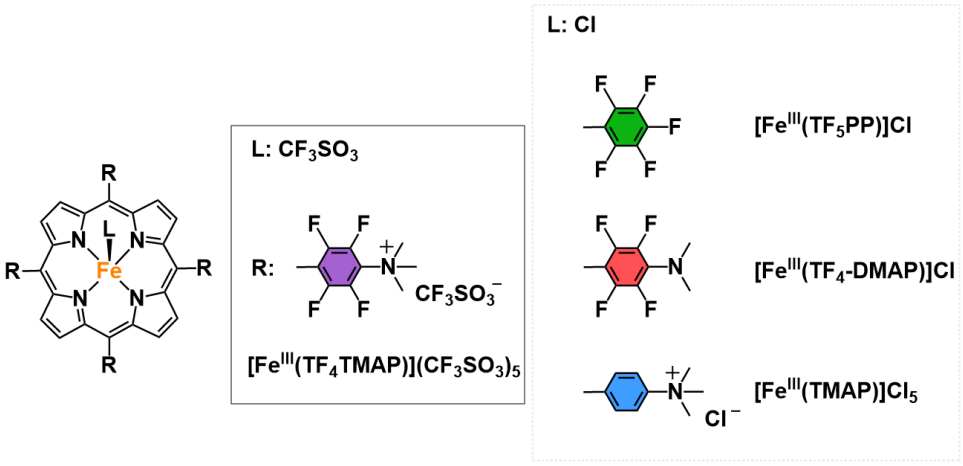

Figure 1: Iron porphyrins studied as catalysts for photocatalytic conversion of CO_2.

RESULTS AND DISCUSSION

Synthesis and Characterization

The preparation of iron porphyrin **[Fe^{III}(TF$_4$TMAP)](CF$_3$SO$_3$)$_5$** was performed following an already published synthetic procedure[31] as is illustrated in Scheme S1. Although the synthesis of this porphyrin was reported in the literature, to the best of our knowledge it has never been tested towards photocatalytic or electrocatalytic transformation of CO_2. Moreover, during the intermediate steps of this synthetic procedure, we isolated the two non-charged reference derivatives **[Fe^{III}(TF$_5$PP)]Cl**

and **[Fe^{III}(TF$_4$-DMAP)]Cl**, that were also examined as catalysts towards photocatalytic CO_2 reduction. The positively charged catalyst **[Fe^{III}(TMAP)]Cl$_5$** was prepared according to the literature.[32] All the final iron catalysts were characterized through ^{1}H and ^{19}F NMR and UV-Vis absorption spectroscopy measurements and the recorded spectra are in accordance with the already reported data. In addition, we performed the magnetic characterization of **[Fe^{III}(TF$_4$TMAP)](CF$_3$SO$_3$)$_5$**, **[Fe^{III}(TF$_4$-DMAP)]Cl** and **[Fe^{III}(TMAP)]Cl$_5$** to get insight into their ground spin states. Figure 2 shows the temperature dependence of the product χ_mT recorded under an applied magnetic field of 1T for the three complexes.

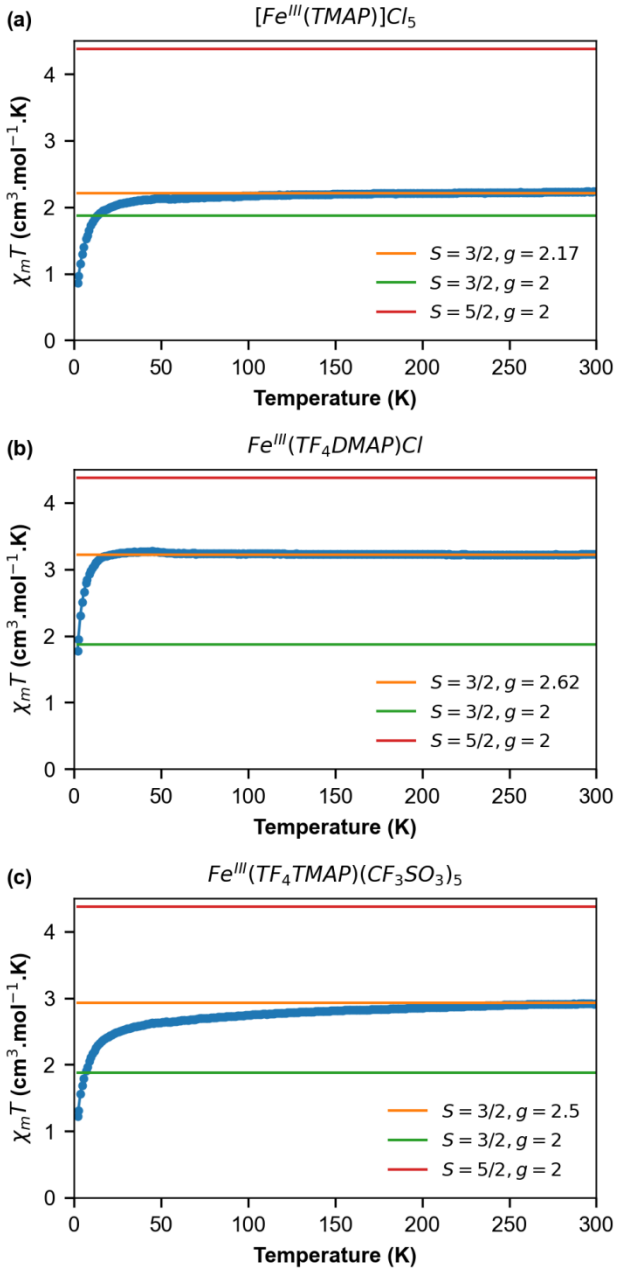

Figure 2: Temperature dependence of $\chi_m T$ for (a) **[Fe^{III}(TMAP)]Cl$_5$**, (b) **[Fe^{III}(TF$_4$-DMAP)]Cl** and (c) **[Fe^{III}(TF$_4$TMAP)](CF$_3$SO$_3$)$_5$** recorded at 1T. The horizontal lines represent the Curie constant expected for an isotropic (g=2), spin S=3/2 (green line) and S=5/2 (red line). The orange line is the best fit at high temperature for S=3/2 and using g as the free parameter.

At room temperature $\chi_m T$ is 2.23 cm^3·mol^{-1}·K, 3.22 cm^3·mol^{-1}·K and 2.91 cm^3·mol^{-1}·K for **[Fe^{III}(TMAP)]Cl$_5$**, **[Fe^{III}(TF$_4$-DMAP]Cl** and **[Fe^{III}(TF$_4$TMAP)](CF$_3$SO$_3$)$_5$** respectively. The expected value for an isotropic (g=2) spin S=3/2 is 1.87 cm^3·mol^{-1}·K (green line) while for a spin S=5/2 is much higher with 4.37 cm^3·mol^{-1}·K. Our measured values of $\chi_m T$ at RT show the orbital contribution of the intermediate Fe^{III} (S=3/2) while the high spin Fe^{III} (S=5/2, 3d^5) is expected to have no orbital contribution. The renormalised g factors are 2.17, 2.62 and 2.5 cm^3·mol^{-1}·K for **[Fe^{III}(TMAP)]Cl$_5$**, **[Fe^{III}(TF$_4$-DMAP)]Cl** and **[Fe^{III}(TF$_4$TMAP)](CF$_3$SO$_3$)$_5$** respectively. The SQUID data support that the three complexes have intermediate spin configuration leading to quartet S=3/2 ground spin state.

The redox properties of **[Fe^{III}(TF$_4$TMAP)](CF$_3$SO$_3$)$_5$** were investigated via cyclic voltammetry (CV) under Ar atmosphere and were compared to the reference compounds. The CVs of all iron porphyrin derivatives displayed three quasi-reversible cathodic waves assigned to the Fe^{III}/Fe^{II} and formal Fe^{II}/Fe^{I} and Fe^{I}/Fe^{0} redox couples [33] (Table 1, Figure S1). As expected, the fluoro-substituted catalysts displayed more positive redox potentials compared to **[Fe^{III}(TMAP)]Cl$_5$**, due to the electro-withdrawing inductive effect of the introduced fluorine groups on the phenyl rings. Interestingly, for **[Fe^{III}(TF$_4$TMAP)](CF$_3$SO$_3$)$_5$** an additional cathodic wave was observed right after the Fe^{II}/Fe^{I} and prior to the Fe^{I}/Fe^{0} redox processes. This probably involves the perfluorinated trimethylanilinium groups, since this behavior was not detected with the unfluorinated analog **[Fe^{III}(TMAP)]Cl$_5$**, or with the fluorinated **[Fe^{III}(TF$_4$-DMAP)]Cl** derivative. Among the investigated iron catalysts, **[Fe^{III}(TF$_4$TMAP)](CF$_3$SO$_3$)$_5$** exhibited the most favorable reduction potentials due to the presence of both fluoro and positively charged trimethylammonium groups. Indeed, methylation of the dimethylamino group shifts the redox potentials at more positive values by almost 200 mV.[31b]

Table 1: Reduction potentials of porphyrin based catalysts. All potentials are reported *vs*. $Fc^{+/0}$ which was used as internal standard.

	Fe^{III}/Fe^{II} [V]	Fe^{II}/Fe^{I} [V]	Fe^{I}/Fe^{0} [V]
$[Fe^{III}(TF_4TMAP)](CF_3SO_3)_5$	-0.23	-1.15	-1.77
$[Fe^{III}(TF_5PP)]Cl$	-0.42	-1.28	-1.79
$[Fe^{III}(TF_4$-DMAP$)]Cl$	-0.46	-1.31	-1.87
$[Fe^{III}(TMAP)]Cl_5$	-0.54	-1.39	-1.86

* *[catalyst]: 0.5 mM, [NBu_4PF_6]: 0.05 M as supporting electrolyte, solvent: DMF, proton source: H_2O (5.5M), scan rate: 0.1 V s^{-1}.*

In a CO_2-saturated solution and in the presence of H_2O (5.5 M), the CVs of **$[Fe^{III}(TF_4TMAP)](CF_3SO_3)_5$** and reference compounds exhibited a great enhancement of the cathodic current at their formal Fe^{I}/Fe^{0} redox couple which was also shifted to more anodic potentials (Figure S2). Such CV response is indicative of CO_2 activation by the formal Fe^0 state of the corresponding catalyst which is considered necessary in order to accomplish the CO_2 binding on the metal center of the porphyrin during catalysis. Thus, the four iron catalysts have the ability to reduce CO_2 and can be utilized for the photocatalytic transformation of CO_2.

Theoretical calculations

Theoretical calculations were performed in the Density Functional Theory framework to get insight into the structures and molecular properties of the Fe porphyrin series. Due to the absence of X-ray crystal structures, we first generated computational model systems for all complexes. The structures of the putative species were then subjected to geometry optimization (see Supporting Information for Cartesian coordinates) and their electronic as well as spectroscopic properties were investigated to be confronted to experimental data. Using the DFT-optimized structures, we performed free energy calculations considering all possible spin states of **$[Fe^{III}(TF_4TMAP)](CF_3SO_3)_5$** to determine its ground spin state (Table S1). Our calculations suggest that the iron center of the complex is in an intermediate spin configuration leading to a quadruplet state (S=3/2) that is favored by more than 10 kcal·mol^{-1} with respect to the doublet (S=1/2) and sextet (S=5/2) states. Interestingly, the same trend is also observed for the other complexes, namely **$[Fe^{III}(TF_5PP)]Cl$**, **$[Fe^{III}(TF_4$-DMAP$)]Cl$** and **$[Fe^{III}(TMAP)]Cl_5$**, for which the quadruplet state is

assigned as the ground spin states as it is found to be energetically more stable in all cases (Tables S2-S4). While a high-spin configuration could have been expected for Fe^{III}-porphyrins, the DFT findings are supported by magnetic susceptibility measurements performed on the complexes that concluded to the quartet S =3/2 being the ground spin state. Time-dependent DFT calculations were then performed on the optimized structure of **$[Fe^{III}(TF_4TMAP)](CF_3SO_3)_5$** to obtain a theoretical estimation of the optical properties of the complex and further support its ground spin state. Our results show that the computed UV/vis spectra of the species is dominated by one intense absorption band at 340 nm and two other transitions found at 420 and 470 nm in agreement with experimental data (Figure S3). The TDDFT-computed spectrum adequately reproduces the key features of the spectrum in terms of energy and intensity, supporting the fact that the complex ground spin state is indeed in a quadruplet state.

Redox potential calculations were also conducted to fully assign the electrochemical events experimentally observed for the four complexes (Tables S1-4) The computed values for the one-, two- and three-electron reduction processes of **$[Fe^{III}(TF_4TMAP)](CF_3SO_3)_5$** are -0.17, -1.19 and -1.71 V versus $Fc^{+/0}$, in fair agreement with the experimental values, which actually indicates that the cathodic system corresponds to a monoelectronic processes (Table 2). Looking at the computed values for the other complexes, our calculations reproduce the experimental trend and support the fact that the presence of fluoro groups combined with charged trimethyl-ammonium groups lead to an anodic shift of the redox potentials since the most positive values are obtained for the **$[Fe^{III}(TF_4TMAP)](CF_3SO_3)_5$** complex while the most negative ones are calculated for the **$[Fe^{III}(TMAP)]Cl_5$**.

Table 2: DFT-computed redox potentials of the catalysts (V *vs*. $Fc^{+/0}$).

	Fe^{III}/Fe^{II} [V]	Fe^{II}/Fe^{I} [V]	Fe^{I}/Fe^{0} [V]
$[Fe^{III}(TF_4TMAP)](CF_3SO_3)_5$	-0.17	-1.19	-1.71
$[Fe^{III}(TF_5PP)]Cl$	-0.65	-1.48	-1.95
$[Fe^{III}(TF_4$-DMAP$)]Cl$	-0.54	-1.36	-1.89
$[Fe^{III}(TMAP)]Cl_5$	-0.77	-1.63	-2.04

Electronic structures of the neutral, one-, and two-electron reduced species of the Fe porphyrin series were computed. The spin density plots of the neutral complexes show that most of the spin density is localized at the iron center as expected for Fe^{III} complexes with a S=3/2 ground spin state. This is further supported by the sets of localized SOMOs that show that the orbitals are Fe 3d-metal based orbitals (Figure S4). Upon one and two-electron reductions, these plots support metal-based electrochemical processes with spin densities remaining localized on the iron centers (Figure S5). For the first reduction, calculations suggest a triplet state, being followed by a doublet after a second reduction, and finishing at a closed-shell singlet for a third subsequent reduction reaction (Table S1-4). It is worth noting that these findings are quite different from thse obtained by Neese and coworkers[33] which can be rationalized by the presence of axial anions coordinated to the metal center within the present series of iron porphyrins. Electronic structure calculations upon successive reductions indeed highlight a non-negligible contribution from the chlorine/triflate anions that helps retaining most of the spin density at the iron center (Figure S5). Such localized distribution of the spin density in the reduced complexes thus prevents any role from the porphyrin ligand leading to subsequent metal-based reduction events. Our calculations all show electronic structures concentrated at the Fe center, suggesting that the reactivity of these complexes is mainly metal-centered.

Photocatalytic Studies

The photocatalytic experiments were carried out in an ACN/ H_2O (98:2 v/v) solvent mixture in the presence of **$[Ir(ppy)_2bpy]PF_6$** (0.2 mM) as the chromophore (Figure S6) and triethylamine (TEA) as the sacrificial electron donor (SED). After 4 h of irradiation, **$[Fe^{III}(TF_4TMAP)](CF_3SO_3)_5$** (2 μM) presented the highest performance, catalyzing the CO_2 reduction to CO with a TON of 341. In contrast, porphyrins **$[Fe^{III}(TF_4\text{-}DMAP)]Cl$** and **$[Fe^{III}(TMAP)]Cl_5$** demonstrated lower activity achieving a TON_{CO} of 282 and 272, respectively. Finally, catalyst **$[Fe^{III}(TF_5PP)]Cl$** showed the lowest activity towards CO_2 reduction with a TON_{CO} of 226 (Figure 3).

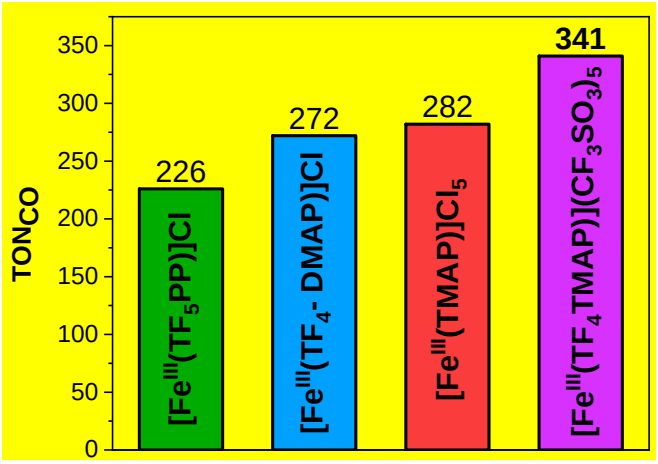

Figure 3: Comparison of the CO production activity in TONs of all iron catalysts. Experiment conditions: ACN-H_2O (98:2 v/v), 2 μM of each iron catalyst, 0.2 mM **[Ir(ppy)$_2$bpy]PF$_6$**, 50 mM TEA after 4 h of irradiation.

The low efficiency of **[Fe^{III}(TF$_5$PP)]Cl** can be attributed to the presence of the fluoro electron-withdrawing substituents that decrease the electron density on the iron center, and therefore its capability to combine with CO_2 in the first step of the catalytic process.[27] Thus, in this case the Fe-CO_2 intermediate cannot be stabilized effectively and the catalysis is suppressed. On the other hand, in the best performing catalyst **[Fe^{III}(TF$_4$TMAP)](CF$_3$SO$_3$)$_5$**, the fluoro-groups shift the reduction potentials to more positive values and at the same time the positively charged trimethyl-ammonium groups enhance the stabilization of the Fe-CO_2 adduct via through-space coulombic interactions as has been previously reported by Azcararate et al.[34] All the above results highlight that **[Fe^{III}(TF$_4$TMAP)](CF$_3$SO$_3$)$_5$** is the most active catalyst due to the simultaneous presence of the fluoro and the trimethyl-ammonium groups. As depicted in Figure S7a, the CO formation ceases after almost 4 h of continuous irradiation.

The readdition of iron catalyst or iridium complex or TEA did not restore the catalytic activity. In contrast, the CO production profile was restored after the concurrent addition of **[Fe^{III}(TF$_4$TMAP)](CF$_3$SO$_3$)$_5$** and **[Ir(ppy)$_2$bpy]PF$_6$**. The degradation of the iron catalyst and the iridium complex is thus concluded to be the major reason for the cease of photocatalysis.

In an effort to improve the catalytic activity we examined the influence of the wavelength of the light source. For the photocatalytic studies a LED ring set-up

(Figure S8) has been applied for the irradiation of the samples. With this set-up we had the ability to change the color of the LED strip in white, blue, green and red. Depending on the color of the LED ring, the emitted light corresponds in different wavelengths. The catalytic studies demonstrated that the light source alters the catalytic efficiency and the highest performance observed with the white light source (Figure 4a). The blue and the green LEDs presented similar activity, while in the case of the red color no CO was detected. The white LED light presents three maxima and due to its broader spectrum is expected to excite the Ir chromophore more efficiently (Figure 4b). Based on these results, all the following experiments were conducted with the white LED ring as the light source.

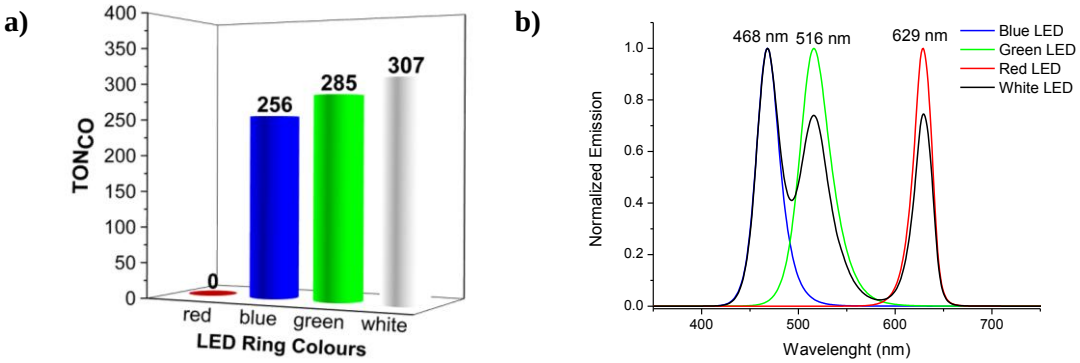

Figure 4: a) CO production depending on the LED color. Experiment conditions: CO_2-saturated ACN:H_2O (99:1 v/v) solution containing 2 μM **[Fe^{III}(TF_4TMAP)](CF_3SO_3)$_5$**, 0.2 mM **[Ir(ppy)$_2$bpy]PF_6** and 50 mM TEA after 4 h of irradiation; b) Emission spectra of each color of the LED ring.

According to the literature, the presence of small amount of water in the catalytic mixture can play a significant role during the CO_2 reduction process, since it can act as a proton source.[35] In detail, addition of 1% water in acetonitrile can increase the yield of CO_2 to CO transformation by 30%. Based on these observations, we examined the influence of the water content in our catalytic system. A wide range of

water percentages (from 0.1% to 20%) was utilized. According to Figure 5a, addition of water results in the enhancement of the catalytic activity. The highest performance (TON = 380) was obtained when 10% water was employed. However, between 2% and 10%, the CO_2 reduction yield remains almost the same (341 to 380 TONs). Therefore, in order to avoid the side unwanted reduction reaction of hydrogen evolution, which is kinetically favored in the presence of H_2O,[8] we continued our catalytic studies utilizing 2% of water in the catalytic system.

The catalytic efficiency of CO_2 reduction is strongly correlated with the catalyst concentration.[36] In an effort to identify the optimum concentration of the catalyst; we kept the amount of the iridium-based chromophore stable (0.2 mM), while the concentration of the iron catalyst was varied from 0.005 μM to 30 mM. As the catalyst concentration decreases, the TON of the produced CO increases exponentially (Figure 5b). Under the optimal conditions ([catalyst] = 0.005 μM), a remarkable activity was obtained, achieving a high TON of about 5500 and a TOF = 1375 h^{-1}. This is among the highest values for CO_2 photocatalytic reduction system employing an iron porphyrin as the catalyst. Further decrease on the catalyst concentration was not examined due the low level of accuracy when very small amounts of produced CO are measured.

a)

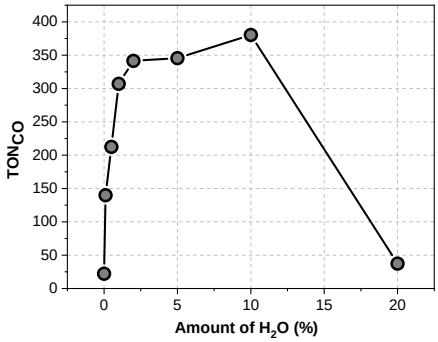

b)

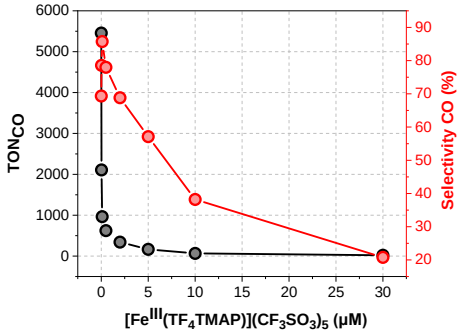

Figure 5: a) CO production by varying in the amount of the water in a CO_2-saturated ACN solution containing 2 μM **[Fe^{III}(TF_4TMAP)](CF_3SO_3)$_5$**, 0.2 mM **[Ir(ppy)$_2$bpy]PF_6** and 50 mM TEA after 4 h of irradiation; b) CO Evolution (TON_{CO}) in CO_2-saturated ACN:H_2O (99:2 v/v) solutions containing various concentrations of **[Fe^{III}(TF_4TMAP)](CF_3SO_3)$_5$**, 0.2 mM **[Ir(ppy)$_2$bpy]PF_6** and 50 mM TEA after 4 h of irradiation. Selectivity of CO_2 reduction vs H_2 evolution of CO_2-saturated solutions of ACN:H_2O (98:2 v/v) containing various concentrations of **[Fe^{III}(TF_4TMAP)](CF_3SO_3)$_5$**, 0.2 mM **[Ir(ppy)$_2$bpy]PF_6** and 50 mM TEA.

Furthermore, numerous control experiments were performed in order to examine the importance of every single constituent in our photocatalytic system. Under the same experimental conditions, in the absence of iron catalyst, only traces of CO were detected, while in absence of light, no CO was detected, meaning that light irradiation is indeed the driving force for this system. Notably, by removing, either the chromophore or the SED, the system is incapable of processing the CO_2 reduction. Therefore, in order to achieve CO production, all the three basic components are necessary.

Apart from **[Ir(ppy)$_2$bpy]PF_6** chromophore, a ruthenium complex (**[Ru(bpy)$_3$](PF_6)$_2$**, Figure S6) was also examined as PS. After irradiation with the white LED, ruthenium chromophore was able to activate the iron catalyst and the formation of CO was observed with a TON of 202 (Figure S9). However, its activity was lower compared to the iridium photosensitizer, which under the same conditions produced CO with a TON of 341. Thus, in this catalytic system the iridium complex seems to be more effective PS compared to the ruthenium derivative. Another parameter that was investigated was the sacrificial agent (Figure S10). When triethanolamine (TEOA) was employed as SED the photocatalytic CO_2 to CO transformation was very low (TON = 32). On the other hand, when 1,3-dimethyl-2-phenyl-2,3-dihydro-1H-benzo[d]imidazole (BIH) was used as SED the catalytic activity was increased compared to TEOA reaching a TON of 201. However, the highest catalytic activity (TON = 341) was obtained when TEA was applied as the sacrificial donor.

As already mentioned, during the CO_2 reduction the undesired side reaction of hydrogen evolution can also take place. During our investigations, hydrogen has been also detected as a side reaction product along with the CO production. Therefore, we

examined the selectivity of **[Fe^{III}(TF$_4$TMAP)](CF$_3$SO$_3$)$_5$** catalyst at various concentrations. As presented in Figure S7b, the selectivity of our system increases at low catalyst concentrations. The maximum selectivity was 86% and observed when the catalyst concentration was 0.1 μM. In addition, under N_2 atmosphere, no CO evolution was observed; in contrast under these conditions hydrogen appeared to be the main product. Moreover, analysis of the ion chromatography failed to detect formate (HCOO−) and therefore there were not any other CO_2 reduction products detected after the photocatalytic experiments.

Mechanistic Studies

In order to examine the mechanism for light-driven CO_2 reduction in our photocatalytic system we carried out quenching experiments of the **[Ir(ppy)$_2$bpy]PF$_6$** excited state by the SED (TEA) and by the iron porphyrin catalyst using Stern–Volmer analysis. At an excitation wavelength of 415 nm, the luminescence of the iridium complex at 590 nm was efficiently quenched by TEA with an apparent quenching rate constant of 11.9 M^{-1} (Figure S11). On the other hand, the fluorescence of the iridium photosensitizer was not particularly attenuated by the iron catalyst (Figure S12). In summary, the major electron transfer pathway occurs from the excited PS to TEA, therefore CO production in our system is initiated via reductive quenching of the PS.

Initially, a photoinduced electron transfer between the PS and TEA occurs, generating the reduced state of PS. Then, the reduced intermediate PS triggers the subsequent reduction of the catalyst, which is activated in order to perform the photo-induced reduction of CO_2 to CO. The proposed reductive quenching mechanism is similar to previously reported system using an iridium complex as the photosensitizer.[37]

EXPERIMENTAL SECTION

Materials and Methods

Reagents and solvents were purchased as reagent grade from usual commercial sources and were used without further purification, unless otherwise stated.

$[Ir(ppy)_2(bpy)]PF_6$ was purchased from commercial sources and used without further purification. The iron catalysts **$[Fe^{III}(TF_5PP)]Cl$**,[38] **$[Fe^{III}(TMAP)]Cl_5$**,[31,32,39] **$[Fe^{III}(TF_4\text{-}DMAP)]Cl$**[31b, 40] and **$[Fe^{III}(TF_4TMAP)](CF_3SO_3)_5$**[31b] were prepared as previously reported in the literature.

SQUID Magnetometry

Magnetic characterization has been performed using a conventional SQUID magnetometer MPMS-XL from Quantum Design working at a magnetic field up to 5 T and temperature down to 2 K. The samples (powder) are filled in polypropylene sleeves then sealed in order to remove the maximum of dioxygen, which give the signal around 50 K (antiferromagnetic transition). Diamagnetic contribution of the sample holder was removed as well as the diamagnetism of for **$[Fe^{III}(TMAP)]Cl_5$** (χ_{dia}= -584x10^{-6} $cm^3 \cdot mol^{-1}$), **$[Fe^{III}(TF_4\text{-}DMAP)]Cl$** ($\chi_{dia}$= -666x$10^{-6}$ $cm^3 \cdot mol^{-1}$) and **$[Fe^{III}(TF_4TMAP)](CF_3SO_3)_5$** ($\chi_{dia}$= -888x$10^{-6}$ $cm^3 \cdot mol^{-1}$).

Electrochemical Studies

Cyclic voltammetry experiments were realized in an electrochemical cell with a conventional three-electrode system; a glassy carbon electrode (3 mm diameter) as the working electrode, a saturated aqueous KCl standard calomel electrode (SCE) as the reference, and a platinum wire as the counter electrode. Extra dry dimethylformamide (DMF, AcroSeal 99.8%) was used as the solvent, while recrystallized tertbutylammonium hexafluorophosphate (NBu_4PF_6) was employed as the supporting electrolyte (0.05 M). The concentration of the investigated compounds was 0.5 mM, whereas ultrapure H_2O was used as the proton source with a resistivity of 18.2 MΩ·cm at 25 °C. Before recording any CV, the working electrode was tactfully polished with a 6 μm diamond paste and successively washed with ethanol and acetone and finally dried. Ferrocenium was used as an internal standard.

Photocatalytic experiments

The photocatalytic experiments were performed in a 11 mL glass vial and each sample was sealed with a silicone septum. The solvent (5 mL) was a mixture of acetonitrile and H_2O and the vials were bubbled with CO_2 for 10 minutes before being irradiated. The gaseous products were determined using gas chromatography with Shimadzu GC 2010 plus chromatograph with a TCD detector and a 5 Å molecular

sieve column (30 m to 0.53 mm). The experiments were performed using a LED ring. This set-up provided defined positions and certain amount (50 W cm^{-2}) of the emitted light for all the vials simultaneously. Each sample was measured by taking the amount of 100 μL from the headspace of the vial and then injecting them into the GC. Provided that the system was appropriately calibrated for CO detection and quantification, the calibration curve allowed the determination of moles of the produced gas. This was succeeded by converting the integration area from the GC data, into moles and turnover numbers accordingly, which were calculated based on the moles of produced CO vs. the moles of the catalyst. Selectivity was calculated according to the equation: Sel_{CO2} = selectivity for CO_2 reduction *vs*. water reduction = mol (CO) / [mol (H_2) + mol (CO)].

Stern-Volmer experiments

In situ solutions of **$[Ir(ppy)_2(bpy)]PF_6$** (0.04 mM) in acetonitrile were prepared containing different concentrations of the catalyst and SED. In the case of TEA, the concentration varied from 2.0 mM to 22.0 mM, while for the iron porphyrin concentrations from 0.04 μM to 0.4 μM were used.

Theoretical calculations

All calculations were performed using the ORCA program package.[41] Full geometry optimizations were carried out for all complexes using the GGA functional BP86[42] in combination with the def2-TZV/P(-f)[43] basis set for all atoms and by taking advantage of the resolution of the identity (RI) approximation in the Split-RI-J variant[44] with the appropriate Coulomb fitting sets.[45] Increased integration grids (Grid4 in ORCA convention) and tight SCF convergence criteria were used. For accordance to the experimental conditions, all calculations including geometry optimizations were performed in acetonitrile solvent by invoking the Control of the Conductor-like Polarizable Continuum Model (CPCM).[46] To ensure that the resulting structures converged to a local minimum on the potential energy surface, frequency calculations were performed and resulted in only positive normal vibrations. The Gibbs free energies were computed from the optimized structures as a sum of electronic energy, solvation and thermal corrections to the free energy. Redox potentials were obtained from the calculated free energy change between oxidized and reduced species in solution. The relative potentials are referenced to the ferrocene

couple and as such, a computed value of 4.87 eV was subtracted to make direct comparisons to experimental data.[47] Electronic structures were obtained from single-point DFT calculations using the hybrid functional B3LYP[48] together with the def2-TZVP-(f) basis set. Optical properties and UV-Vis spectra were predicted from additional single-point calculations using the def2-TZV/P basis in combination with the range-separated hybrid GGA functional CAM-B3LYP.[49] Vertical electronic transitions were calculated using time-dependent DFT within the Tamm-Dancoff approximation (TDA).[50] To increase computational efficiency, the RI approximation[51] was used in calculating the Coulomb term, and at least 30 excited states were calculated in each case. Spin density plots, molecular orbitals as well as difference density plots for each transition were generated using the orca plot utility program and were visualized with the Chemcraft program.[52]

CONCLUSIONS

In conclusion, we have developed an efficient photocatalytic CO_2 reduction system, using an appropriately substituted iron porphyrin (**[Fe^{III}(TF$_4$TMAP)](CF$_3$SO$_3$)$_5$**) as catalyst. CO was produced selectively in the presence of **[Ir(ppy)$_2$bpy]PF$_6$** as photosensitizer and TEA as electron donor. We also inspected the catalytic activity of three reference iron catalysts (**[Fe^{III}(TF$_5$PP)]Cl**, **[Fe^{III}(TF$_4$-DMAP)]Cl** and **[Fe^{III}(TMAP)]Cl$_5$** to verify the efficiency of our catalyst. Moreover, various parameters such as the light source, H_2O concentration, nature of the SED, nature of the PS and the concentration of catalyst, were examined in order to determine the optimal conditions of the system. Therefore, the TON and TOF reached 5500 and 1375 h^{-1}, respectively, which are among the highest values reported for iron porphyrins in the photocatalytic CO_2 reduction in homogenous systems. The high catalytic efficiency can be attributed to the synergistic effect of the electron-withdrawing nature of fluorine groups and the positively charged groups' stabilization towards CO_2 coordination. Mechanistic studies have also shown the reductive quenching of the excited state of the PS, whom intermediate causes the electron transfer to the catalyst. The iron catalyst is then activated and fulfills the requirements to proceed the CO_2 reduction, showing excellent turnover numbers and selectivity towards CO.

ACKNOWLEDGEMENTS

This research was funded by the General Secretariat for Research and Technology (GSRT) and Hellenic Foundation for Research and Innovation (HFRI; project code: 508). This research has been co-financed by the European Union and Greek national funds through the Regional Operational Program "Crete 2014-2020," project code OPS:5029187. Moreover, the European Commission's Seventh Framework Program (FP7/2007-2013) under grant agreement no. 229927 (FP7-REGPOT-2008-1, Project BIO-SOLENUTI) and the Special Research Account of the University of Crete are gratefully acknowledged for the financial support.

REFERENCES

[1] W. Wu, X. Ma, Y. Zhang, W. Li, Y. Wang, *Sci. Total Environ.* **2020**, *707*, 135447.
[2] S. D. Kenarsari, D. Yang, G. Jiang, S. Zhang, J. Wang, A. G. Russell, Q. Wei, M. Fan, *RSC Adv.* **2013**, *3*, 22739-22773.
[3] a) R. Francke, B. Schille, M. Roemelt, *Chem. Rev.* **2018**, *118*, 4631-4701; b) H.-R. M. Jhong, S. Ma, P. J. A. Kenis, *Curr. Opin. Chem. Eng.* **2013**, *2*, 191-199.
[4] a) R. Lin, J. Guo, X. Li, P. Patel, A. Seifitokaldani, *Catalysts* **2020**, *10*, 473; b) X. Zhang, S.-X. Guo, K. A. Gandionco, A. M. Bond, J. Zhang, *Mater. Today Adv.* **2020**, *7*, 100074.
[5] a) Y.-X. Pan, Y. You, S. Xin, Y. Li, G. Fu, Z. Cui, Y.-L. Men, F.-F. Cao, S.-H. Yu, J. B. Goodenough, *J. Am. Chem. Soc.* **2017**, *139*, 4123-4129; b) M. Muringa Kandy, A. Rajeev K, M. Sankaralingam, *Sustain. Energy Fuels* **2021**, *5*, 12-33.
[6] M. F. Demirbas, *Energy Sources, Part A* **2007**, *29*, 563-569.
[7] a) Y. Kuramochi, Y. Fujisawa, A. Satake, *J. Am. Chem. Soc.* **2019**, *142*, 705-709; b) M. F. Kuehnel, K. L. Orchard, K. E. Dalle, E. Reisner, *J. Am. Chem. Soc.* **2017**, *139*, 7217-7223; c) Y. Li, D. Hui, Y. Sun, Y. Wang, Z. Wu, C. Wang, J. Zhao, *Nat. Commun.* **2021**, *12*.
[8] N. Elgrishi, M. B. Chambers, M. Fontecave, *Chem. Sci.* **2015**, *6*, 2522-2531.
[9] F. Wang, *ChemSusChem* **2017**, *10*, 4393-4402.
[10] Y. Yamazaki, H. Takeda, O. Ishitani, *J. Photochem. Photobiol., C* **2015**, *25*, 106-137.
[11] C. Du, X. Wang, W. Chen, S. Feng, J. Wen, Y. A. Wu, *Mater. Today Adv.* **2020**, *6*, 100071.
[12] L. Chen, Z. Guo, X.-G. Wei, C. Gallenkamp, J. Bonin, E. Anxolabéhère-Mallart, K.-C. Lau, T.-C. Lau, M. Robert, *J. Am. Chem. Soc.* **2015**, *137*, 10918-10921.
[13] a) R. Küngas, *J. Electrochem. Soc.* **2020**, *167*, 044508; b) H.-K. Wu, F. Zhang, J.-Y. Li, Z.-R. Tang, Y.-J. Xu, *J. Mater. Chem. A* **2020**, *8*, 24253-24266.
[14] H. Takeda, K. Koike, H. Inoue, O. Ishitani, *J. Am. Chem. Soc.* **2008**, *130*, 2023-2031.

[15] P. Kang, T. J. Meyer, M. Brookhart, *Chem. Sci.* **2013**, *4*, 3497-3502.
[16] H. Takeda, H. Koizumi, K. Okamoto, O. Ishitani, *Chem. Commun.* **2014**, *50*, 1491-1493.
[17] Z. Guo, F. Yu, Y. Yang, C.-F. Leung, S.-M. Ng, C.-C. Ko, C. Cometto, T.-C. Lau, M. Robert, *ChemSusChem* **2017**, *10*, 4009-4013.
[18] X. Zhang, K. Yamauchi, K. Sakai, *ACS Catal.* **2021**, *11*, 10436-10449.
[19] H. Rao, C.-H. Lim, J. Bonin, G. M. Miyake, M. Robert, *J. Am. Chem. Soc.* **2018**, *140*, 17830-17834.
[20] Y. Okabe, S. K. Lee, M. Kondo, S. Masaoka, *JBIC J. Biol. Inorg. Chem.* **2017**, *22*, 713-725.
[21] S. Fukuzumi, Y.-M. Lee, H. S. Ahn, W. Nam, *Chem. Sci.* **2018**, *9*, 6017-6034.
[22] C. Costentin, G. Passard, M. Robert, J.-M. Savéant, *J. Am. Chem. Soc.* **2014**, *136*, 11821-11829.
[23] L. Zou, R. Sa, H. Lv, H. Zhong, R. Wang, *ChemSusChem* **2020**, *13*, 6323– 6329
[24] P. Gotico, Z. Halime, A. Aukauloo, *Dalton Trans.* **2020**, *49*, 2381-2396.
[25] E. Nikoloudakis, I. Lopez-Duarte, G. Charalambidis, K. Ladomenou, M. Ince, A. G. Coutsolelos, *Chem. Soc. Rev.* **2022**, *51*, 6965-7045
[26] E. Pugliese, P. Gotico, I. Wehrung, B. Boitrel, A. Quaranta, M. H. Ha-Thi, T. Pino, M. Sircoglou, W. Leibl, Z. Halime, A. Aukauloo, *Angew. Chem. Int. Ed.* **2022**, *61*, e202117.
[27] I. Azcarate, C. Costentin, M. Robert, J.-M. Savéant, *J. Phys. Chem. C* **2016**, *120*, 28951-28960.
[28] H. Rao, J. Bonin, M. Robert, *ChemSusChem* **2017**, *10*, 4447-4450.
[29] H. Rao, L. C. Schmidt, J. Bonin, M. Robert, *Nature* **2017**, *548*, 74-77.
[30] H. Rao, J. Bonin, M. Robert, *J. Phys. Chem. C* **2018**, *122*, 13834-13839.
[31] aT. La, G. M. Miskelly, R. Bau, *Inorg. Chem.* **1997**, *36*, 5321-5328; bT. La, R. Richards, G. M. Miskelly, *Inorg. Chem.* **2002**, *33*, 3159-3163.
[32] A. Kalilur Rahiman, K. Shanmuga Bharathi, S. Sreedaran, V. Narayanan, *Catal. Lett.* **2008**, *127*, 175-182.
[33] C. Römelt, S. Ye, E. Bill, T. Weyhermüller, M. van Gastel, F. Neese, *Inorg. Chem.* **2018**, *57*, 2141-2148.
[34] I. Azcarate, C. Costentin, M. Robert, J.-M. Savéant, *J. Am. Chem. Soc.* **2016**, *138*, 16639-16644.
[35] J. Grodkowski, D. Behar, P. Neta, P. Hambright, *J. Phys. Chem. A* **1997**, *101*, 248-254.
[36] a) T. Ouyang, H. H. Huang, J. W. Wang, D. C. Zhong, T. B. Lu, *Angew. Chem. Int. Ed.* **2016**, *56*, 738-743; b) D. Hong, Y. Tsukakoshi, H. Kotani, T. Ishizuka, T. Kojima, *J. Am. Chem. Soc.* **2017**, *139*, 6538-6541; c) S. L.-F. Chan, T. L. Lam, C. Yang, S.-C. Yan, N. M. Cheng, *Chem. Commun.* **2015**, *51*, 7799-7801.
[37] A. Rosas-Hernández, P. G. Alsabeh, E. Barsch, H. Junge, R. Ludwig, M. Beller, *Chem. Commun.* **2016**, *52*, 8393-8396.
[38] a) N. Ono, H. Kawamura, M. Bougauchi, K. Maruyama, *Tetrahedron* **1990**, *46*, 7483-7496; b) S. Rebelo, A. Silva, C. Medforth, C. Freire, *Molecules* **2016**, *21*, 481-492.
[39] C. Ruzié, P. Even, D. Ricard, T. Roisnel, B. Boitrel, *Inorg. Chem.* **2006**, *45*, 1338-1348.
[40] K. M. Kadish, B. C. Han, M. M. Franzen, C. Araullo-McAdams, *J. Am. Chem. Soc.* **2002**, *112*, 8364-8368.
[41] F. Neese, *WIREs Comput. Mol. Sci.* **2011**, *2*, 73-78.

[42] a) J. P. Perdew, *Phys. Rev. B* **1986**, *34*, 7406-7406; b) J. P. Perdew, *Phys. Rev. B* **1986**, *33*, 8822-8824; c) A. D. Becke, *Phys. Rev. A* **1988**, *38*, 3098-3100.
[43] A. Schäfer, C. Huber, R. Ahlrichs, *J. Chem. Phys.* **1994**, *100*, 5829-5835.
[44] F. Neese, *J. Comput. Chem.* **2003**, *24*, 1740-1747.
[45] F. Weigend, *Phys. Chem. Chem. Phys.* **2006**, *8*, 1057-1065.
[46] V. Barone, M. Cossi, *J. Phys. Chem. A* **1998**, *102*, 1995-2001.
[47] A. Barrozo, M. Orio, *ChemSusChem* **2019**, *12*, 4905-4915.
[48] a) A. D. Becke, *J. Chem. Phys.* **1993**, *98*, 1372-1377; b) C. Lee, W. Yang, R. G. Parr, *Phys. Rev. B* **1988**, *37*, 785-789.
[49] T. Yanai, D. P. Tew, N. C. Handy, *Chem. Phys. Lett.* **2004**, *393*, 51-57.
[50] a) M. E. Casida, *Recent Advances in Density Functional Methods;* Recent Advances in Computational Chemistry, World Scientific, **1995**, *1*, 155-192; b) R. E. Stratmann, G. E. Scuseria, M. J. Frisch, *J. Chem. Phys.* **1998**, *109*, 8218-8224; c) R. Bauernschmitt, R. Ahlrichs, *Chem. Phys. Lett.* **1996**, *256*, 454-464; d) S. Hirata, M. Head-Gordon, *Chem. Phys. Lett.* **1999**, *314*, 291-299; e) S. Hirata, M. Head-Gordon, *Chem. Phys. Lett.* **1999**, *302*, 375-382.
[51] F. Neese, *J. Chem. Phys.* **2001**, *115*, 11080-11096.
[52] M. Joseph, S. Haridas, *Int. J. Hydrogen Energy* **2020**, *45*, 11954-11975.